Catalysis Letters
https://doi.org/10.1007/s10562-018-2366-8

Aluminium Oxide Supported on SBA-15 Molecular Sieves as Potential Lewis Acid Catalysts for Epoxide Ring Opening Using Aniline

Rekha Yadav[1] · Akhila Muralidhar[2] · A. Shamna[2] · P. Aghila[2] · Lakshmiprasad Gurrala[3] · Ayyamperumal Sakthivel[2]

Received: 8 February 2018 / Accepted: 15 March 2018

Abstract

A series of aluminium oxide (Al_2O_3)-supported SBA-15 molecular sieves were prepared using a one-step wet-impregnation method. Powder X-ray diffraction, nitrogen adsorption/desorption, infrared spectroscopy and ammonia TPD were used to investigate the structures and chemical natures of the surface-bound species. The FT-IR studies of metal-impregnated SBA-15 materials revealed strong covalent interaction of Al_2O_3 on SBA-15 materials with strong Lewis acidic properties, evident from ammonia-TPD studies. The metal oxide-supported SBA-15 catalysts are active for epoxide ring opening with aniline at room temperature, and showed remarkably high stability and selectivity towards mono-alkylated products (about 86%) viz., 1-(phenylamino)propan-2-ol and 2-(phenylamino)propan-1-ol. The catalytic activities remained intact after several recycles. The observed activities and selectivities were compared with other metal oxide-loaded SBA-15 catalysts obtained by similar preparation methods.

Graphical Abstract

Aluminium oxide supported SBA-15 molecular sieves were prepared using a one-step wet-impregnation method. The materials showed strong Lewis acidic sites and promising catalytic activity for epoxide ring opening with aniline at room temperature.

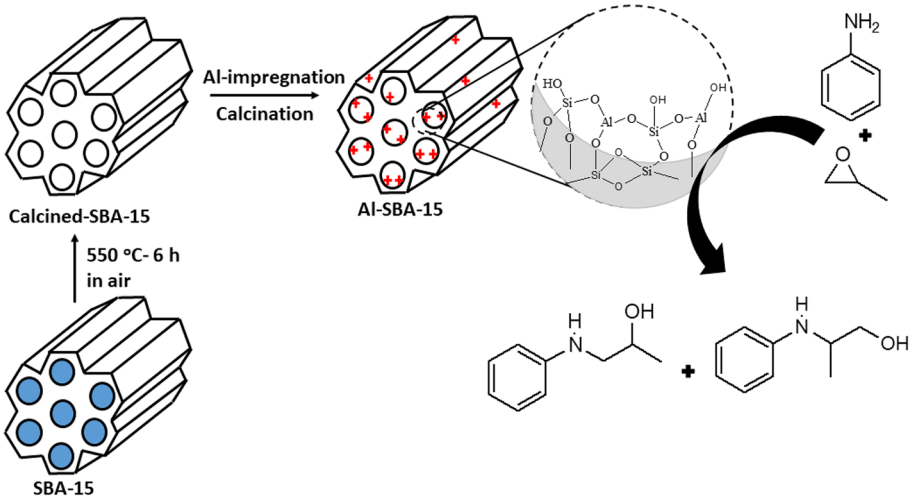

Keywords Epoxide ring opening · Kinetics · β-Amino alcohol · Al_2O_3-SBA-15 · Molecular sieves

Akhila Muralidhar and A. Shamna have equally contributed to this work.

Extended author information available on the last page of the article

Published online: 22 March 2018

1 Introduction

Catalysts play an important role in day-to-day life by contributing to various chemical and environmental processes [1, 2]. In particular, heterogeneous catalysts e.g. zeolite and zeolite-like molecular sieves are extensively used in various petrochemical processes such as fluidised catalytic cracking (FCC) [3], refining, Friedel–Crafts alkylation, hydroisomerisation, methanol to gasoline, polymerisation, condensation, etc. [3–6]. However, the small pore size of zeolites restricts their use for bulky molecular transformations. The pore size constraints of zeolite materials were addressed by development of mesoporous molecular sieves possessing wider pore diameters in the range of 2–50 nm, high surface area (1000–1500 $m^2\ g^{-1}$), uniform framework channels, excellent sorption capacity (1 $cm^3\ g^{-1}$), etc. [7–9]. In particular, a substantial amount of work has focused on the Santa Barbara Amorphous (SBA-15) materials developed by Stucky et al. [9], due to their unique characteristic features, including excellent thermal and hydrothermal stability, thick pore walls, highly ordered structural regularity and simple synthesis method and reproducibility [10–12]. The pure silica-based SBA-15 framework, however, lacks surface acidity, basicity or redox properties, which limits its catalytic applications. The introduction of hetero-elements into the guest framework of SBA-15 resulted in a wide variety of applications, including catalysis, absorbance and potential support [13–15]. In particular, the introduction of a metal oxide such as aluminium oxide (Al_2O_3) into the framework by a post-synthesis method facilitates the generation of Lewis acidic sites, which have shown potential acid catalysis in various reactions [12, 16, 17].

At this junction, it is important to note that epoxides are widely utilised as synthetic intermediates and are considered as 'Spring-loaded' rings for nucleophilic ring opening resulting in versatile intermediates in organic synthesis [18–23]. The epoxide ring opening yields β-substituted alcohols, which have tremendous application as organic intermediates [23, 24]. It will be interesting to develop a versatile heterogeneous catalyst for such processes. Thus, the present work focuses on the preparation of aluminium oxide supported on SBA-15 and utilises it for β-amino alcohol formation by epoxide ring opening with aniline under ambient reaction conditions. For comparison, ZnO and Fe_2O_3 loaded SBA-15 were prepared using similar processes and their catalytic activities were compared under identical conditions.

2 Experimental

2.1 Synthesis of Al-SBA-15

The SBA-15 was synthesized as per literature [11, 24] described elsewhere with molar gel composition 6.89×10^{-4} P123 triblock copolymers: 0.24 HCl:0.041 TEOS:7.88 H_2O. Aluminum oxide is introduced into SBA-15 using wet impregnation method [25]. Calculated amount of $Al(NO_3)_3$ required to get 5, 10 and 20 wt% of Al_2O_3 on SBA-15 support (1.25 g) was introduced and the resultant materials was calcined at 550 °C for 6 h in an air oven. The sample prepared with 5, 10 and 20 wt% Al_2O_3 were represented as Al-SBA-15-5, Al-SBA-15-10, and Al-SBA-15-20 respectively. Similarly, 20 wt% of iron oxide and zinc oxide were loaded using $Fe(NO_3)_3$ as iron precursor and $Zn(NO_3)_3$ as zinc precursor and are represent as Fe-SBA-15-20 and Zn-SBA-15-20 respectively [26].

2.2 Characterization

All the samples were systematically characterized using analytical and spectroscopic techniques. The wide angle powder X-ray diffraction patterns were obtained with a Rigaku Mini flex 600 diffractometer using nickel-filtered Cu-Kα radiation (λ = 1.54184 Å) and a liquid nitrogen cooled germanium solid-state detector. The diffracto-grams were recorded in the 2θ ranges of 5°–60° with a scan speed and step size of 4°/min and 0.02 respectively. While low angle powder X-ray diffraction patterns of different samples were recorded using 18 kW XRD Rigaku (2500 V), Japan with Cu-Kα radiation (λ = 1.54184 Å) in the 2θ ranges of 0.5°–6° with scan speed and step size of 0.5° and 0.02 min^{-1} respectively.

FT-IR spectra were obtained using Perkin-Elmer FT-IR SPECTRUM TWO in the range 400–4000 cm^{-1} using KBr pellets. The textural properties (BET surface area, micropore area (t-plot method), BJH average pore volume etc.) of the samples were derived from N_2 adsorption–desorption measurements carried out at − 196 °C using automatic micropore physisorption analyser (Micromeritics 2020) after the samples were degassed at 150 °C for at least 10 h prior to each run. Thermogravimetry-analysis (TGA) was carried out in a thermal analyser (Perkin-Elmer STA6000) in air. About 0.5–0.6 mg of the sample was taken in the alumina pan and heated in air in temperature range of 50–800 °C at the rate of 20 °C min^{-1}.

2.3 Catalytic Studies

The different metal oxide loaded SBA-15 were studied for propylene oxide ring opening using aniline (Scheme 1). In a

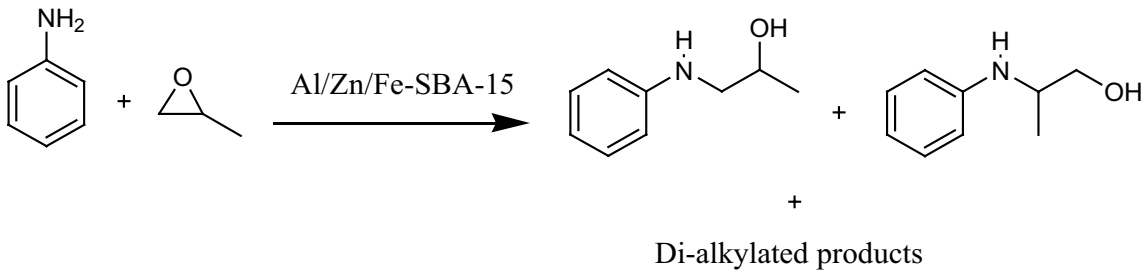

Scheme 1 Schematic representation of ring opening of propylene oxide with aniline using metal-oxide loaded SBA-15 catalysts

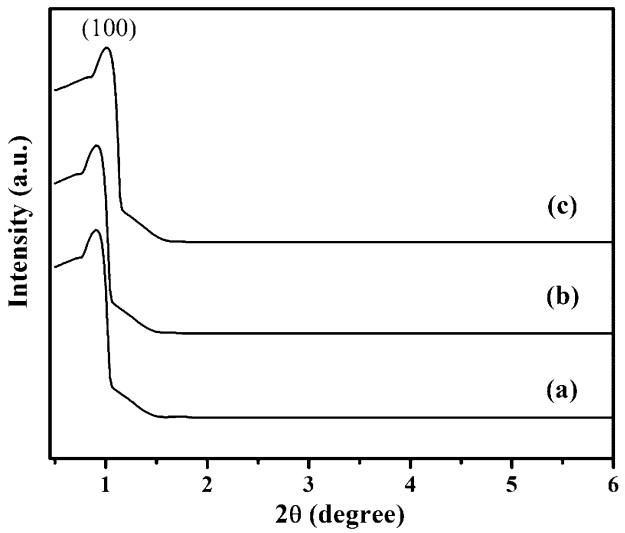

Fig. 1 Low-angle powder XRD of (*a*) Al-SBA-15-20, (*b*) Zn-SBA-15-20, and (*c*) Fe-SBA-15-20

typical reaction, aniline and propylene oxide (10 mmol each) were taken in a round bottom flask with 60 mg of catalyst under constant stirring without solvent for one hour at 45 °C. The reaction was also studied in different experimental conditions including temperature, reactant ratios, different epoxide as substrate. After reaction, the products were extracted with calculated amount of propanol and analysed using gas chromatography (Agilent 7890A series) equipped with HP-5 capillary column.

3 Result and Discussion

The low-angle XRD patterns of calcined parent SBA-15 (Fig. 1) and different metal-loaded SBA-15 materials are displayed in Fig. 1. The low-angle XRD pattern of calcined SBA-15 exhibits three well resolved peaks at 2θ of 0.67°, 1.3° and 1.5°, indexed to diffraction planes (100), (110) and (200), respectively (not shown here) [27, 28]. The resulting Bragg reflections confirmed the hexagonal symmetry (P6mm) of the SBA-15 material [27]. The intense peak corresponding to plane (100) (2θ of 0.67) indicates the long-range ordering. The calcined SBA-15 impregnated with 20 wt% metal oxides showed much broader peaks centred at 2θ of 0.89, 0.91 and 1.0 for Al, Zn and Fe respectively (Fig. 1). The prominent similarity in the X-ray diffraction peaks suggests the retention of hexagonal structure even after a large amount of metal oxide introduction. The broadening in the peaks owing to the introduction of large amounts of bulk oxide inside the mesoporous channels results in shift of X-ray reflection towards the higher angles. The higher-angle XRD patterns of all the samples showed a broad peak ranging from 2θ = 15°–30° due to the presence of amorphous silica walls, and the absence of any peaks corresponding to metal oxides (Fig. 2A) [17, 29]. The above observation clearly indicates that even at very high loading (20 wt%) there is no X-ray reflection for Al_2O_3, suggesting that metal oxides are uniformly distributed in the SBA-15 channels. Similarly, no segregation of metal oxides on the sample prepared using zinc oxide and/or iron oxide-loaded samples (Fig. 2B) suggests well dispersed metal oxides on the SBA-15 surface.

FT-IR spectra of Al_2O_3 loaded SBA-15 and different metal-loaded SBA-15 samples were recorded in the infrared region from 400 to 4000 cm^{-1} (Fig. 3). The broad band centred around 3400 cm^{-1} in all materials was due to the stretching vibration of surface hydroxyl group [10]. The presence of C–H bond stretching was confirmed by peaks appearing around 2900 cm^{-1}, which are characteristic of the polymer hydrocarbon [30, 31]. All these peaks disappeared after calcination (Fig. 3B), indicating the complete removal of template. The as-synthesised Al-SBA-15 samples showed (Fig. 3A) a sharp peak around 1300 cm^{-1} corresponding to nitrate species derived from the aluminium nitrate precursor. The three typical Si–O–Si peaks centred at 1100 cm^{-1} (asymmetric stretching), 800 cm^{-1} (symmetric stretching), and 450 cm^{-1} (bending) were assigned to the condensed silica network. The vibrational bands appearing around 1087 and 1096 cm^{-1} in both as-prepared and calcined sample correspond to as-symmetric stretching of Si–O–Si and Si–O–Al respectively. For the metal oxide-loaded materials, the band

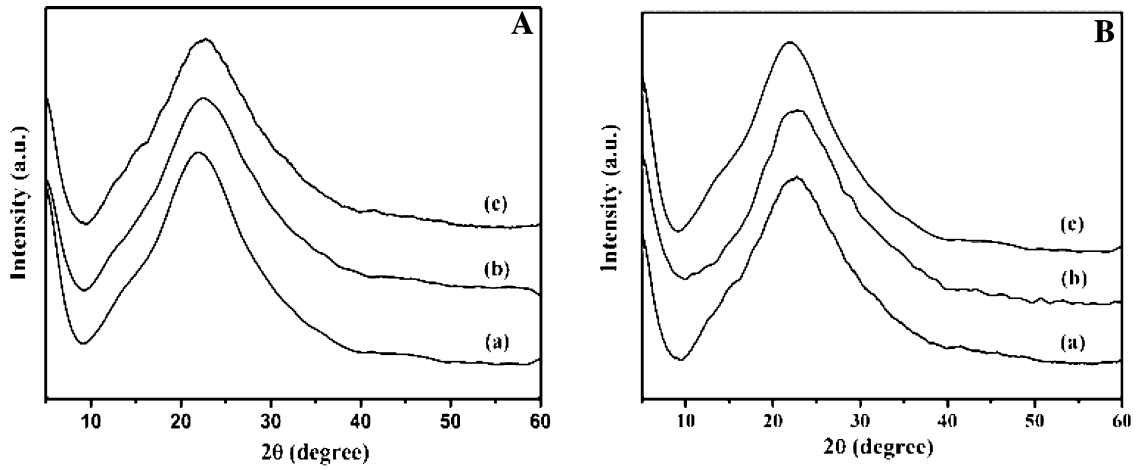

Fig. 2 Wider-angle **A** powder XRD pattern of (*a*) Al-SBA-15-5, (*b*) Al-SBA-15-10, (*c*) Al-SBA-15-20 and **B** powder XRD pattern of (*a*) Al-SBA-15-20, (*b*) Zn-SBA-15-20, (*c*) Fe-SBA-15-20

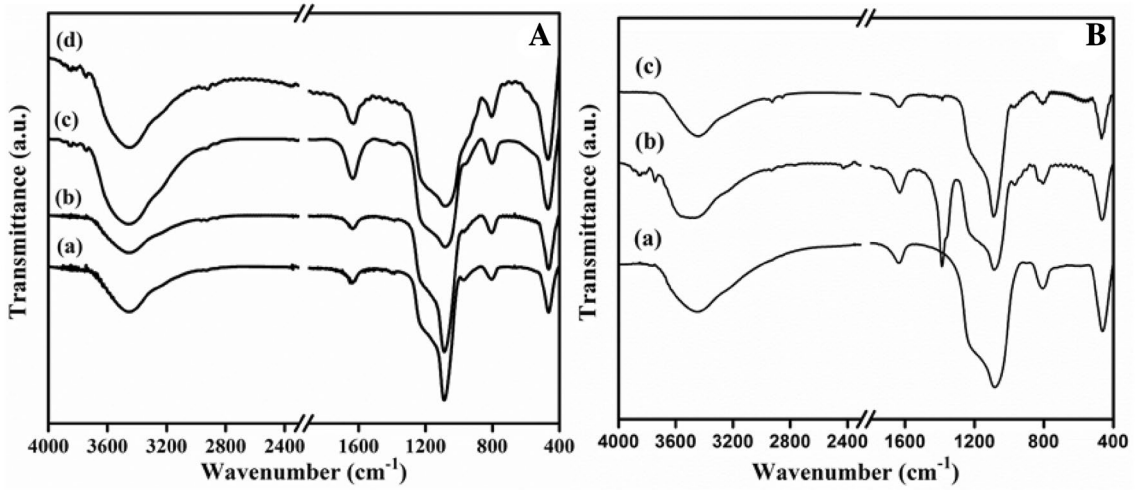

Fig. 3 FT-IR spectra for calcined **A** (*a*) SBA-15, Al_2O_3 loaded SBA-15 materials (*b*) Al-SBA-15-5, (*c*) Al-SBA-15-10, (*d*) Al-SBA-15-20 and **B** different metal oxide loaded SBA-15 (*a*) Al-SBA-15-20, (*b*) Zn-SBA-15-20, (*c*) Fe-SBA-15-20

at 960 cm^{-1} is ascribed to Si–O–X (X = Al, Zn and Fe) stretching vibration (Fig. 3), indicating metal oxide covalently incorporated into the SBA-15 framework [26, 32, 33].

The textural properties of different metal oxide-loaded SBA-15 samples measured by N_2 sorption and the corresponding isotherms are displayed in Fig. 4. Figure 4A depicts the N_2 adsorption desorption isotherm of SBA-15 and Al_2O_3-supported SBA-15 materials. The BET surface area of the parent SBA-15 was found to be in the range of 769 $m^2\ g^{-1}$ with a pore volume of 1.1 $cm^3\ g^{-1}$. A well-defined adsorption step at relative high pressure of 0.6–0.8 was observed, corresponding to capillary condensation of N_2, indicating uniformity of the pores. According to the IUPAC classification, all isotherms are of type IV and exhibit a hysteresis loop, typical of large-pore mesoporous solids. The isotherms of different metal loaded SBA-15 feature well-defined hysteresis loops [34–36]. The specific structural parameters are given in Table 1. The BET surface area of the modified samples decreased compared with that of the calcined SBA-15, which suggested the incorporation of Al_2O_3 particles into the pore channels of SBA-15. Similarly, Fig. 4B depicts the N_2 adsorption desorption isotherm of different metal oxide supported SBA-15 materials. All isotherms are of type IV and exhibit a hysteresis loop indicating the presence of uniform mesopores.

Figure 5A displays the pore size distribution of SBA-15 and Al_2O_3-loaded SBA-15 materials. The parent SBA-15 shows a uniform distribution of pore size in the range of

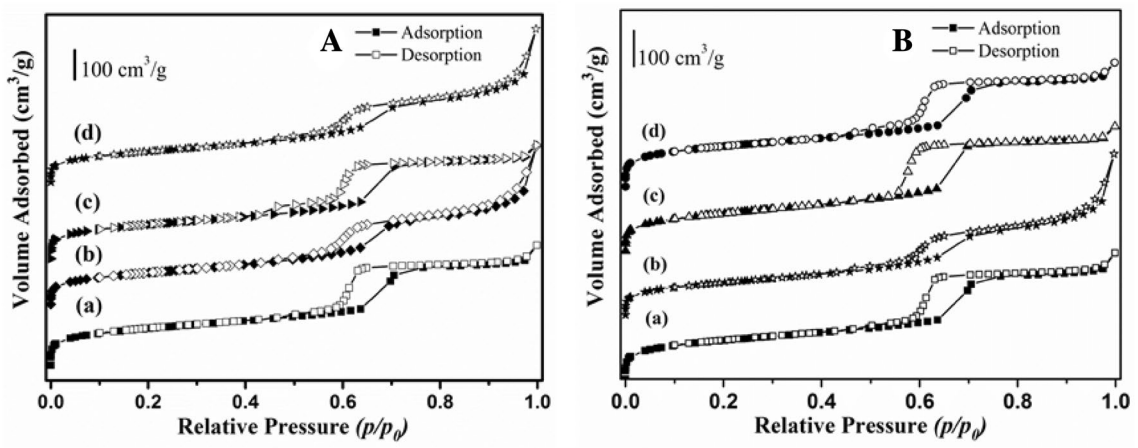

Fig. 4 N_2 adsorption isotherm **A** (*a*) SBA-15, Al_2O_3 loaded SBA-15 materials (*b*) Al-SBA-15-5, (*c*) Al-SBA-15-10, (*d*) Al-SBA-15-20 and **B** (*a*) SBA-15, different metal oxide-loaded SBA-15 (*b*) Al-SBA-15-20, (*c*) Zn-SBA-15-20, (*d*) Fe-SBA-15-20

Table 1 Textural properties of Al_2O_3 loaded SBA-15 materials

Catalyst	Surface area (m^2/g)	Acidity (mmol)		Pore volume (cm^3/g)	
	BET	Moderate	Strong	t-plot micropore	BJH
SBA-15	769	–	–	0.018	1.100
Al-SBA-15-5	364	1.05	0.52	0.015	0.792
Al-SBA-15-10	386	–	–	0.026	0.562
Al-SBA-15-20	355	1.58	4.92	0.015	0.762
Fe-SBA-15-20	431	0.33	2.45	0.598	0.047
Zn-SBA-15-20	406	1.11	2.50	0.021	0.587

5.3 nm, whereas Al-SBA-15 shows a broad distribution of pore size centred at 5.2 nm, possessing inter-particle mesoporosity derived from the impregnated Al_2O_3 present in the Al-SBA-15 samples. The pore size distribution displays a bimodal distribution typical of cage-type mesoporous structures. Compared to calcined SBA-15, a decrease in the primary mesoporous cage structure diameter (5.2 nm) is noted for metal oxide-loaded samples. Similarly, Fig. 5B shows the pore size distribution for different metal oxides. A sharp decrease in surface area and pore volume is observed for different metal oxide-loaded materials, with pore sizes of 5.2, 5.0 and 5.2 nm for Al-SBA-15-20, Zn-SBA-15-20 and Fe-SBA-15-20 respectively compared to parent calcined SBA-15 material [12].

The surface acidity of different metal oxide-loaded SBA-15 (Fig. 6) was qualitatively measured using ammonia

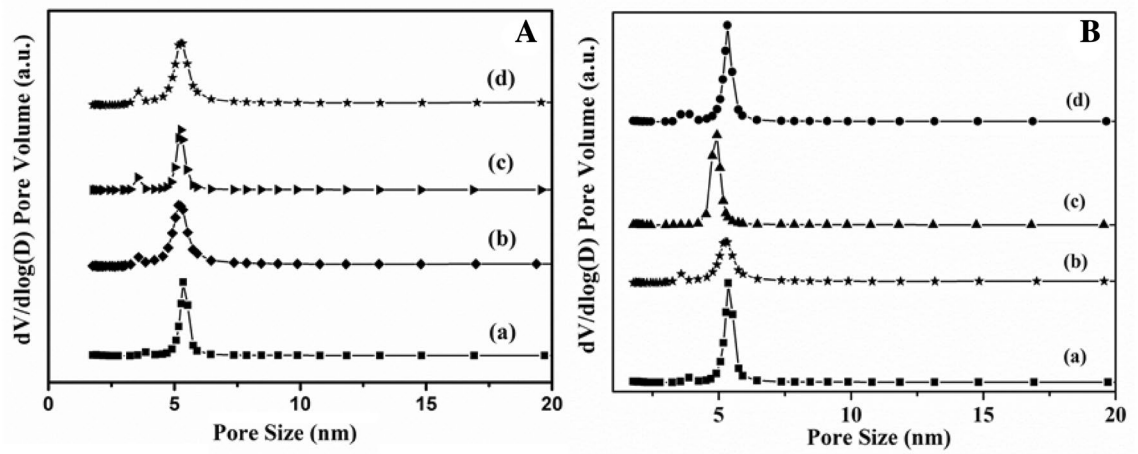

Fig. 5 Pore size distribution of materials **A** (*a*) SBA-15, Al_2O_3 loaded SBA-15 materials (*b*) Al-SBA-15-5, (*c*) Al-SBA-15-10, (*d*) Al-SBA-15-20 and **B** (*a*) SBA-15, different metal oxide loaded SBA-15 (*b*) Al-SBA-15-20, (*c*) Zn-SBA-15-20, (*d*) Fe-SBA-15-20

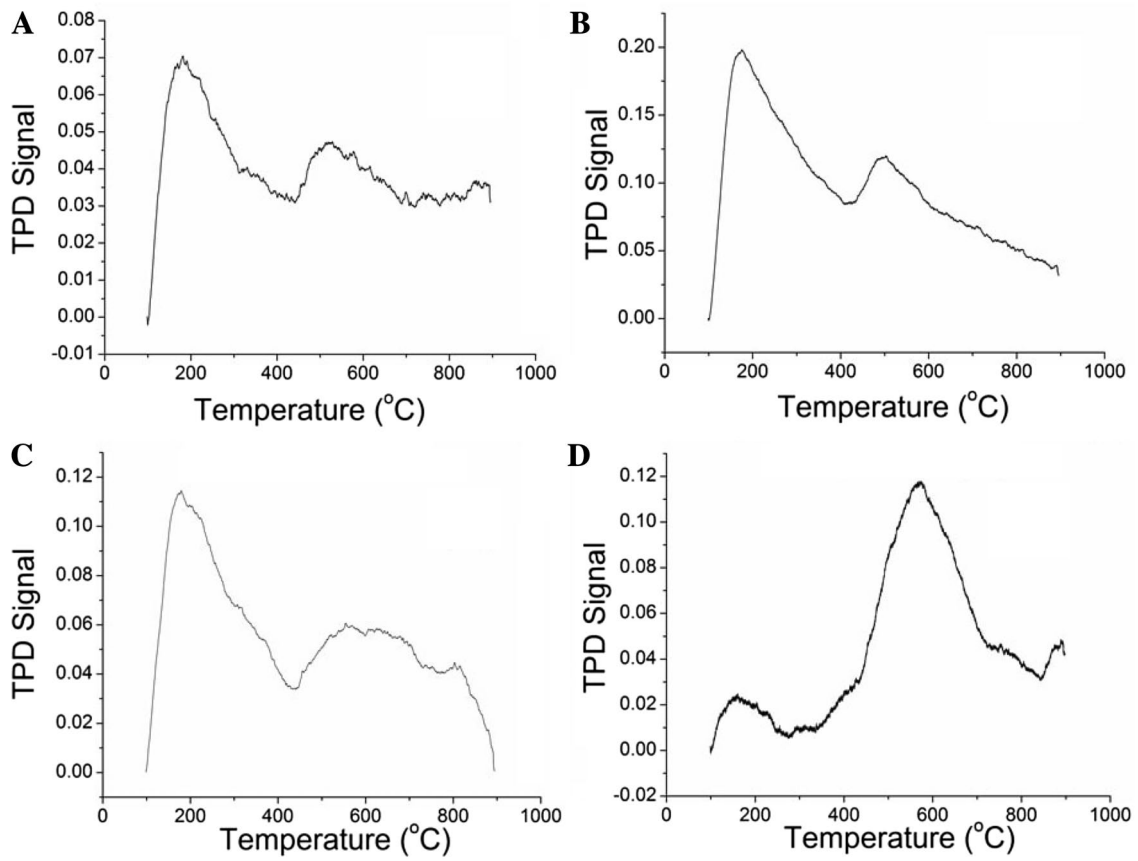

Fig. 6 TPD of **A** Al-SBA-15-5, **B** Al-SBA-15-20, **C** Zn-SBA-15-20 and **D** Fe-SBA-15-20

TPD. The NH_3-TPD profile for all catalysts shows two distinct broad peaks in the temperature range of 100–400 and 400–800 °C, which are assigned to weak and to moderate-to-strong acidic sites respectively [37]. The samples Al-SBA-15-5 and Al-SBA-15-20 possess similar types of peaks; however, the areas under the curves are different. Compared to other metal oxides, Al_2O_3-impregnated samples possess greater numbers of relatively weak acidic sites. The number of moderate acidic sites follows in the order Al-SBA-15-20 > Zn-SBA-15-20 > Fe-SBA-15. Similarly, the number of moderate-to-strong acidic sites follows the same order i.e. Al-SBA-15-20 > Zn-SBA-15-20 > Fe-SBA-15-20. Hence, in comparison to other materials, Al-SBA-15-20 exhibits a greater number of weak, as well as moderate-to-strong, acidic sites.

4 Catalytic Studies

Metal-loaded SBA-15 catalyst was used for epoxide ring opening using amine for the preparation of β-amino alcohols (Scheme 1). The products are important intermediates in fine-chemical industries. Normally epoxide ring opening is carried out at high temperatures using conventional acid–base catalysts. Hence, it becomes difficult to synthesise β-amino alcohols from low-boiling epoxides. In the present work, different metal oxide-impregnated materials were used for epoxide ring opening at lower temperatures [19, 20]. In all cases, mono-alkyl derivatives of aniline–1-(phenylamino) propan-2-ol and 2-(phenylamino)propan-1-ol were obtained as major products. Figure 7 shows the aniline conversion using Al-SBA-15-5 catalyst at different temperatures. The conversion of aniline increases with increase in temperature, with increased selectivity towards the di-alkylated product; however, above 45 °C only a slight increase in the conversion was evident. Thus, for further studies, all the reactions were carried out at 45 °C. The maximum conversion evident at 45 °C was 69.5, with 85.9 and 14% selectivity towards mono-alkylated and di-alkylated products, respectively.

The concentration of aniline to propylene oxide was varied at 45 °C to study the effect of the ratio. The catalytic activity of Al-SBA-15-5 with varying ratio (aniline/propylene oxide) is displayed in Fig. 8. It is evident that the use of lower propylene oxide concentration results in moderate conversion, with exclusive formation of mono-alkylated product. With an increase in the aniline/propylene

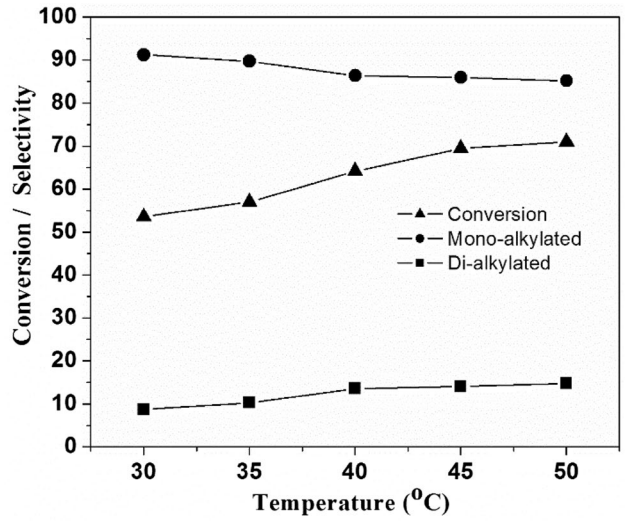

Fig. 7 Effect of reaction temperature on aniline conversion using Al-SBA-15-5 catalyst. Reaction conditions: aniline: propylene oxide = 1:1 (10 mmol each), catalyst = 60 mg, t = 1 h

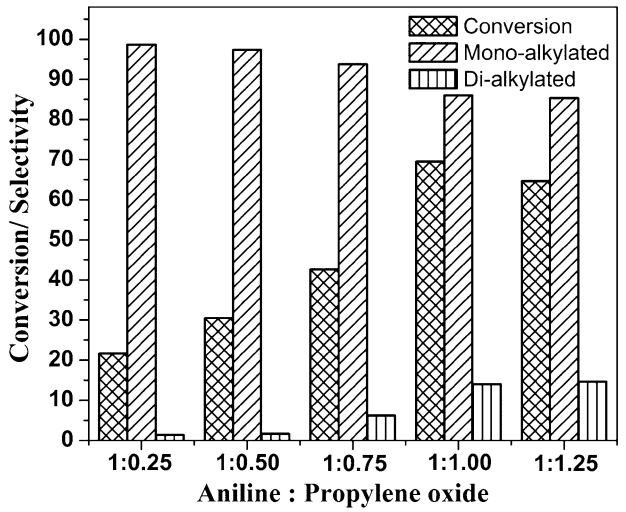

Fig. 8 Effect of change in ratio (aniline/propylene oxide) over Al-SBA-15-5 catalyst. Reaction conditions: catalyst = 60 mg, T = 45 °C, t = 1 h

oxide ratio from 1:0.50 to 1:0.75, enhanced catalytic conversion was observed, which increased further at 1:1 ratio and reached a maximum of 69.48%, with 14.02% selectivity towards di-alkylated products. Further increase in the ratio to 1:1.25 resulted in a decrease in conversion (64.63%) with a slight increase in the selectivity towards di-alkylated products. The decrease in the conversion with increase in the propylene oxide might be due to the adsorption of propylene oxide onto the active sites of the catalysts [20]. Hence, for the further studies, a 1:1 ratio of aniline/propylene oxide was used.

Table 2 Effect of different amount of metal loading on cal-SBA-15

Catalyst	Conversion	Mono-alkylated	Di-alkylated
Without catalyst	2.4	100	–
Cal-SBA-15	33.4	100	–
Al-SBA-15-5	69.5	86.0	14.0
Al-SBA-15-10	58.8	91.2	8.8
Al-SBA-15-20	48.1	92.9	7.1
Fe-SBA-15-20	38.6	93.9	6.1
Zn-SBA-15-20	51.0	94.9	5.1
Recycle Al-SBA-15-5	65.3	86.2	13.8

Reaction conditions: aniline:propylene oxide = 1:1 (10 mmol each), catalyst = 60 mg, T = 45 °C, t = 1 h

Table 2 summarises the catalytic activities of Al_2O_3, ZnO and Fe_2O_3 loaded SBA-15 materials studied at 45 °C with an aniline/propylene ratio of 1:1. Without catalyst, only 2.40% aniline conversion was observed, which increased to about 33.4% with parent calcined SBA-15. The pure SBA-15 having surface hydroxyl group which have weak acidity thus leads to considerable conversion with exclusive formation of mono-N-alkylated products. The introduction of Al_2O_3, ZnO and Fe_2O_3 facilitates to generate moderate-to-strong acidic sites (Fig. 6), thus facilitate improved conversion with the formation of mono-alkylated and considerable di-alkylated products. The conversion level decreased with an increase in Al_2O_3 concentration, and a maximum was reached with Al-SBA-15-5 (about 69.5%). The decrease in the conversion with increase in the Al content might be due to hindering of the active sites of the catalyst and to the greater number of moderate-to-strong acidic sites. The reaction was further carried out on different metal-loaded SBA-15 materials. The conversion followed the order Al-SBA-15-5 > Al-SBA-15-10 > Al-SBA-15-20 ≈ Zn-SBA-15-20 > Fe-SBA-15-20. The higher conversion observed in case of Al-SBA-15-5 might be due to presence of more number of moderate acidic site which facilitates better conversion than other catalyst. The comparable conversion obtained on Al-SBA-15-20 and Zn-SBA-15-20 may be due to presence of strong acidic sites along with moderate acidic sites and thus facilitate secondary reaction. The observed low conversion on Fe-SBA-15-20 might be due to the presence of less moderate acidic sites. The presence of relatively strong acidic sites on Al-SBA-15-20 and Zn-SBA-15-20 facilitates the secondary reaction and thus favour considerable amount of dialkylated product formations. After the catalytic reaction, the catalyst was washed with methanol, dried and reused under optimum reaction conditions. It was evident that the catalytic activity remains intact even after the recycling exercise, with a slight decrease in conversion.

To further examine the catalytic strength of the Al-SBA-15-5 catalyst, different epoxides were used, and

Table 3 Effect of different epoxides on catalytic behaviour of Al-SBA-15-5

Different epoxides	Conversion	Mono-alkylated	Di-alkylated
Propylene oxide	69.5	86.0	14.0
Cyclohexene oxide	58.1	100.0	–
Epi-chloro-hydrine	33.2	95.9	4.1
1,2-Epoxyoctane	33.2	98.2	1.8

Reaction conditions: aniline:epoxide = 1:1 (10 mmol each), catalyst = 60 mg, T = 45 °C; t = 1 h

the results are summarised in Table 3. The conversion with different epoxides followed the order propylene oxide > cyclohexene oxide > 1,2-epoxyoctane ≈ epichlorohydrin. The increase in bulkiness of the substrate results in steric hindrance, which results in relative decrease in catalytic conversion.

5 Conclusion

This is the first time that aluminium oxide loaded SBA-15 materials have been applied to epoxide ring opening using aniline under moderate reaction conditions. The FT-IR studies revealed the covalent interaction of Al_2O_3 on SBA-15 materials, which resulted in strong Lewis acidic sites, evident from ammonia-TPD studies. The aluminium oxide loaded onto SBA-15 materials showed a decrease in X-ray crystallinity, surface area and pore volume, supporting the aluminium oxide being impregnated in the channels of mesoporous SBA-15 molecular sieves. The absence of sharp peaks in high-angle XRD evidenced no segregation of Al_2O_3. The catalyst showed excellent conversion, with selective formation of mono-alkyated product. The catalyst yielded best conversion within one minute, and the catalytic activity remained constant after recycling.

Acknowledgements Authors thanks DST-SERB (EMR-001214) and Central University of Kerala, India is acknowledged for their support.

References

1. Sakthivel A, Selvam P (2002) Catal Lett 84(1):37
2. Primo A, Garcia H (2014) Chem Soc Rev 43(22):7548
3. Herbst JA, Owen H, Schipper PH (1989) Fluidized catalytic cracking process utilizing a C3-C4 paraffin-rich Co-feed and mixed catalyst system with selective reactivation of the medium pore silicate zeolite component thereof. Patent US 4863585
4. Zaera F (2013) Chem Soc Rev 42(7):2746
5. Sartori G, Maggi R (2006) Chem Rev 106(3):1077
6. Chen NY (1996) Shape selective catalysis in industrial applications. CRC Press, New York
7. Pastore HO, Coluccia S, Marchese L (2005) Annu Rev Mater Res 35:351
8. Chen S-Y, Tang C-Y, Chuang W-T, Lee J-J, Tsai Y-L, Chan JCC, Lin C-Y, Liu Y-C, Cheng S (2008) Chem Mater 20(12):3906
9. Wu Z, Zhao D (2011) Chem Commun 47(12):3332
10. Zhao D, Feng J, Huo Q, Melosh N, Fredrickson GH, Chmelka BF, Stucky GD (1998) Science 279(5350):548
11. Zhao D, Sun J, Li Q, Stucky GD (2000) Chem Mater 12(2):275
12. Li Y, Zhang W, Zhang L, Yang Q, Wei Z, Feng Z, Li C (2004) J Phys Chem B 108:9739
13. Tsoncheva T, Ivanova L, Rosenholm J, Linden M (2009) Appl Catal B 89(3):365
14. Lu Q, Tang Z, Zhang Y, Zhu XF (2010) Ind Eng Chem Res 49(6):2573
15. Crisci AJ, Tucker MH, Lee MY, Jang SG, Dumesic JA, Scott SL (2011) ACS Catal 1(7):719
16. Kumaran GM, Garg S, Soni K, Kumar M, Sharma LD, Rama Rao KS, Dhar GM (2007) Ind Eng Chem Res 46(14):4747
17. Rayo P, Ramírez J, Rana MS, Ancheyta J, Aguilar-Elguézabal A (2008) Ind Eng Chem Res 48(3):1242
18. Singh AK, Yadav R, Sakthivel A (2013) Microporous Mesoporous Mater 181:166
19. Yadav R, Ahmed M, Singh AK, Sakthivel, A (2016) Sci Rep 6:22813
20. Ahmed M, Yadav R, Sakthivel A (2016) J Nano Sci Nano Technol 16(9):9298
21. Singh AK, Yadav R, Sudarsan V, Kishore K, Upadhyayula S, Sakthivel A (2014) RSC Adv 4(17):8727
22. Baskaran T, Joshi A, Kamalakar G, Sakthivel A (2016) Appl Catal A 524:50
23. Ahmed M, Sakthivel A (2018) J Porous Mater. https://doi.org/10.1007/s10934-018-0598-z
24. Ager DJ, Prakash I, Schaad DR (1996) Chem Rev 96(2):835
25. Zeng S, Blanchard J, Breysse M, Shi Y, Shu X, Nie H, Li D (2005) Microporous Mesoporous Mater 85:297
26. Barik S, Badamali SK, Sahoo S, Behera N, Dapurkar SE (2018) J Nano Sci Nano Technol 18(1):323
27. Klimova T, Reyes J, Gutiérrez O, Lizama L (2008) Appl Catal A 335(2):159
28. Wang J, Liu Q (2008) Solid State Commun 148(11):529
29. Ren R, Ma J (2015) RSC Adv 5(91):74802
30. Xie W, Hu L, Yang X (2015) Ind Eng Chem Res 54(5):1505
31. Ding Y, Dan H, Dong X, Xian Q, Wang Y, Lu X (2017) Mater Chem Phys 192:156
32. Badoga S, Dalai AK, Adjaye J, Hu Y (2014) Ind Eng Chem Res 53(6):2137
33. Cabrera-Munguia DA, González H, Gutiérrez-Alejandre A, Rico JL, Huirache-Acuña R, Maya-Yescas R, Rosa E (2017) Catal Today 282:195
34. Gómez-Cazalilla M, Mérida-Robles JM, Gurbani A, Rodríguez-Castellón E, Jiménez-López A (2007) J Solid State Chem 180(3):1130
35. Kruk M, Jaroniec M (2001) Chem Mater 13:3169
36. Sing KS (1985) Pure Appl Chem 57(4):603
37. Li C, Wang Y, Guo Y, Liu X, Guo Y, Zhang Z, Wang Y, Lu G (2007) Chem Mater 19(2):173

Affiliations

Rekha Yadav[1] · Akhila Muralidhar[2] · A. Shamna[2] · P. Aghila[2] · Lakshmiprasad Gurrala[3] · Ayyamperumal Sakthivel[2]

✉ Ayyamperumal Sakthivel
sakthivelcuk@cukerala.ac.in

[1] Department of Chemistry, Inorganic Materials & Catalysis Laboratory, University of Delhi, Delhi 110007, India

[2] Department of Chemistry, School of Physical Sciences, Central University of Kerala, Riverside Transit Campus, Kasaragod, Kerala 671314, India

[3] Catalysis and Inorganic Chemistry Division, Council of Scientific and Industrial Research-National Chemical Laboratory (CSIR-NCL), Dr. Homi Bhabha Road, Pune 411008, India